D. Van Lewen, C. Wang, H.C. Lee, A. Devaiah, U. Upahhyay, and S. Russo, "Capacitive Origami Sensing Modules for Measuring Force in a Neurosurgical, Soft Robotic Retractor", in the 2024 International Conference on Robotics and Automation (ICRA 2024).

Capacitive Origami Sensing Modules for Measuring Force in a Neurosurgical, Soft Robotic Retractor

Daniel Van Lewen[1], Catherine Wang[2], Hun Chan Lee[1], Anand Devaiah[3], Urvashi Upadhyay[3], and Sheila Russo[1,2]

***Abstract*— In neurosurgery, soft robots have the potential to introduce significant benefits over traditional metal tools for their ability to safely interact with delicate tissues. In this paper, we introduce a proof-of-concept soft, capacitive origami sensing module (OSM) that can measure forces during neurosurgical retraction. Using origami-inspired design and fabrication principles, the OSM is easily folded and integrated within a soft robotic retractor that interacts with brain tissue to generate a surgical workspace upon actuation. We demonstrate the individual OSM signal response to forces and folding. We further characterize the OSM response within a fully-assembled soft robotic retractor to both folding and the application of forces over 0-5 N showing a 0.38 N average prediction error and resolution of 0.25 N. The sensing capability of the retractor is validated on an in-vitro model to demonstrate prediction errors of 0.06 N and the proposed operation during neurosurgery.**

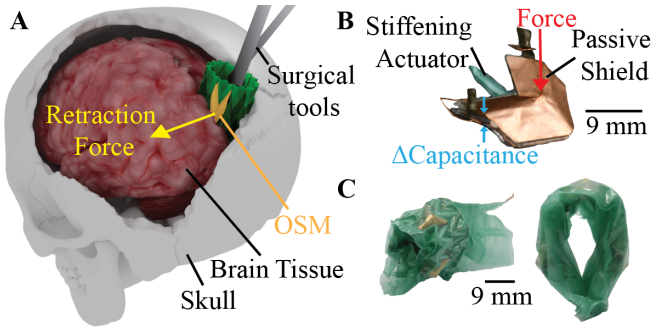

Fig. 1. A) Envisaged use of the sensorized soft robotic retractor displacing and monitoring force applied to brain tissue while creating a path for surgical tools insertion. B) A single origami sensing module (OSM). C) The soft robotic retractor with integrated OSMs in contracted and expanded states.

I. Introduction

During deep-seated brain tumor treatment, neurosurgeons have to remove hard-to-reach tumors by navigating through delicate brain tissue [1]. Healthy tissues are displaced (i.e., retracted) usually through the use of rigid, metal spatulas to allow for tools to be passed into the skull and surgeries such as tumor resection to be performed [2]. Brain cancers are estimated to cause 18,990 deaths in 2023 in the United States [3]. Obtaining safe access to tumors can be a key factor in treatment of these cancers. Modern retraction systems attempt to mitigate retraction related injuries by minimizing localized stress [4]. However, high intracranial pressures between 15-25 mmHg ($\approx$ 2-3.3 kPa) applied over long duration may reduce cerebral blood flow and cause injury [5]. Applied retraction forces can increase pressures beyond this range and cause neurological complications when applied over sustained durations due to lack of monitoring [6], [7]. Further, rigid tool-tissue interactions modeled in the brain have been shown to require up to 2.5 N [8]. In a study of aneurysm treatment procedures, brain retraction injury occurrence was greater than estimated with 16% of patients experiencing new neurological complications as a result [9].

Neurosurgical robotics has primarily focused on improving precision, accuracy, and navigational assistance during procedures [10]–[13]. Robot-assistance in neurosurgery has demonstrated the potential to enhance the surgeon's capabilities [14]. The Robotic Stereotactic Assistance (ROSA) system has decreased lesion tissue biopsy procedures and deep brain stimulation duration through precise localization [15], [16]. Continuum robots have been developed for enabling navigation through tortuous paths such as the skull base or vasculature [17]–[19]. Soft robots have been shown to leverage inherently safe tissue interactions in the brain to deploy electrocorticography arrays [20] and to distribute retraction forces through origami-inspired soft actuation [21].

To enhance soft actuation mechanisms, soft sensors have been developed relying on principles of resistive, optical, and capacitive sensing [22]–[24]. The addition of force sensing has allowed for monitoring of tissue interactions in various procedures. A soft robot for cardiac ablation utilized a soft resistive sensor to successfully measure forces applied on the heart wall [25]. Optical force sensing has recently been applied to colonoscopies, demonstrating the ability to sense contact forces between the colon wall and colonoscope via changes in light intensity [26]. Soft capacitive force sensors have demonstrated potential in electronic skin applications [27]–[30]. In addition, capacitive force sensing in forceps used for minimally invasive surgeries have been successfully validated for feedback on grip forces [31]. Soft, foldable actuators have also readily integrated capacitive

[1]D. Van Lewen, H. Lee, and S. Russo are with the Department of Mechanical Engineering, Boston University, Boston, MA 02215 (USA)

[2]C. Wang and S. Russo are with the Division of Materials Science and Engineering, Boston University, Boston, MA 02215 (USA)

[3]A. Devaiah and U. Upadhyay are with the School of Medicine, Boston University, Boston, MA 02118 (USA)

This publication was supported by the National Center for Advancing Translational Sciences, National Institutes of Health, through Boston University Clinical & Translational Science Institute Grant Number 1UL1TR001430. Its contents are solely the responsibility of the authors and do not necessarily represent the official views of the National Institutes of Health.

Corresponding author E-mail:russos@bu.edu.

D. Van Lewen, C. Wang, H.C. Lee, A. Devaiah, U. Upahhyay, and S. Russo, "Capacitive Origami Sensing Modules for Measuring Force in a Neurosurgical, Soft Robotic Retractor", in the 2024 International Conference on Robotics and Automation (ICRA 2024).

sensing for proprioception in soft surgical robots [32].

In our previous work [21], we introduced an origami-inspired, soft robotic retractor for brain tissue manipulation. Herein, we present the design, fabrication, and modeling of capacitive origami soft sensing modules and their integration into the soft robotic retractor to monitor force output onto the brain during tissue retraction (Fig. 1). The origami sensing modules (OSM) (Fig. 1B) are made foldable and readily integrated into a Miura origami (Miura-ori) pattern of the robot through layer-by-layer fabrication techniques. The elliptical Miura-ori pattern is fully actuated allowing it to contract under vacuum pressures so that it can be inserted into a compact neurological environment and expanded to retract tissue and create a surgical workspace through which the surgeon can pass tools (Fig. 1, A and C). Three OSMs embedded on the retractor's major and minor axes of expansion are calibrated to monitor forces applied to the surroundings when the retractor is expanded. Positive pneumatic pressure enables stiffening of individual Miura-ori unit cells thereby sustaining the applied force. The integration of OSMs into the soft robotic retractor aims to improve the safety of tissue retraction by informing the level of force imparted on brain tissue and therefore, introducing the concept of intraoperative force control to the surgeon.

II. Materials and Methods

A. Design

1) Origami Sensing Module: The OSM is designed with an overall target range of 0-3 N and resolution of 0.3 N to effectively detect potential damaging forces applied on brain tissue [8]. Capacitive sensing in the OSM is achieved by embedding a composite dielectric between two conductive copper plates of 0.045 mm thickness. The complete layering schematic is shown in Fig. 2A. Using 2D layers as shown, enables a batch fabrication method (Fig. 3) to be employed. The conductive plates are cut to the shape of a single Miura-ori unit cell allowing the OSM to follow the folding behavior of the pattern. A unit of Miura-ori pattern fits within a square of dimensions 14.25×16.25 mm, shown in Fig. 2B, and has a surface area of 162 mm^2. Folding behavior is reinforced by layering flexible and structural (0.05 mm thick) Mylar on the outer surface of each electrode. A passive shielding mechanism is included over the Mylar layer on the tissue-facing side of the sensor to reduce parasitic capacitance effects on the OSM (Fig. 2A). The dielectric layer comprises a thermoplastic elastomer (TPE) and Teflon fluidic stiffening actuator surrounded by an Ecoflex 00-50 (Smooth-On, USA) coating. Fluidic TPE actuators have been proven to be effective in origami-inspired robots for their 2D layering designs [33]–[36]. The stiffening actuator enclosed within the OSM, as seen in Fig. 2B, takes the same Miura shape and has an area of 37 mm^2. The overall thickness of the OSM dielectric is 0.68 mm with the Ecoflex 00-50 accounting for 0.55 mm of thickness. Through the use of thin biocompatible layers, capacitive sensing is readily integrated within the origami pattern while maintaining its ability to fold.

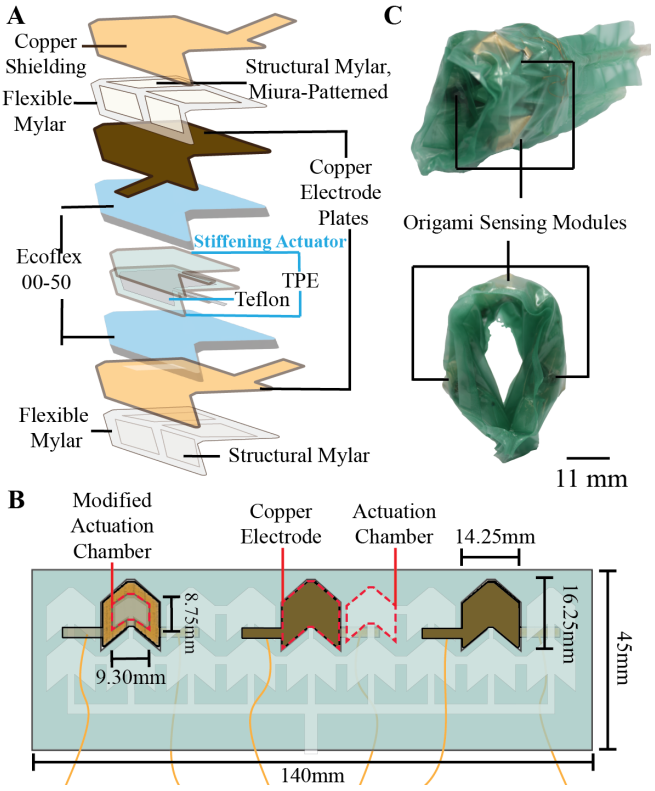

Fig. 2. Origami sensing module design. A) Overview of layers used in the OSM. B) Location and dimensions of OSM and stiffening actuators in pre-wrapped state. C) When the soft robotic retractor is wrapped in its elliptical shape, OSMs are located on the major and minor axes.

2) Sensing Integration with Origami Pattern: We previously demonstrated the concept of integrating fluidic actuation of an origami pattern for application in neurosurgery [21]. The Miura-ori pattern of the robot is wrapped into an elliptical configuration to allow for the passage of surgical instruments through its central channel following the retraction of tissue. Integration of the OSM into the origami pattern was determined based on the major and minor axes of expansion. Therefore, three OSMs were integrated: one on the major axis and one on each end of the minor axis (Fig. 2C). An array of fluidic actuation for each Miura unit cell is embedded within a 45×140 mm layer of Miura-ori patterned Mylar. The actuation layer is outlined with three modified stiffening actuators along its width for placement of each OSM (Fig. 2B). Each stiffening actuator is encased by the Ecoflex 00-50 dielectric using our 2D fabrication method. Therefore, the layering order seen in the individual OSMs is preserved when the pattern is extended to the full size of the retractor. An outer TPE layer surrounds the resulting set of layers so that, by applying vacuum, contraction of the pattern can be controlled (Fig. 2C). To monitor force along each axis, minor axis OSMs are wired in series and the major axis OSM is monitored separately.

B. Fabrication

A layer-by-layer fabrication technique utilizes manual alignment of various layers described in the previous section

D. Van Lewen, C. Wang, H.C. Lee, A. Devaiah, U. Upahhyay, and S. Russo, "Capacitive Origami Sensing Modules for Measuring Force in a Neurosurgical, Soft Robotic Retractor", in the 2024 International Conference on Robotics and Automation (ICRA 2024).

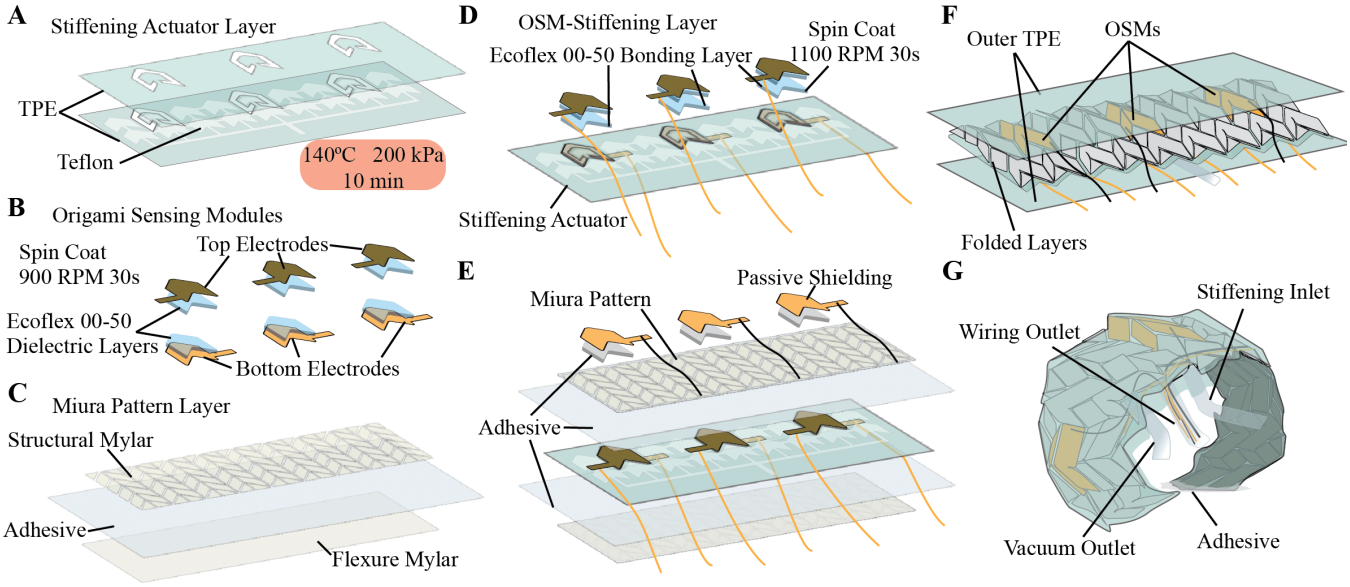

Fig. 3. Fabrication of the soft robotic retractor with integrated force sensing. A) The stiffening actuation layer is heat pressed to create a network of pneumatic chambers. B) Six copper electrodes are spin coated with the elastomer dielectric. C) Miura pattern is guided by stacked, laser cut layers of Mylar. D) The six electrodes are integrated with the stiffening actuator. Another spincoated layer on the top electrodes bonds them to the bottom electrodes. E) The Mylar Miura pattern and passive shielding is integrated over the OSM-stiffening layer via pressure sensitive adhesive. F) The adhered layers are folded and sealed within an outer TPE layer. G) The full assembly is wrapped into an elliptical configuration and fixed with flexible adhesive.

to create the sensorized soft robotic retractor. All layers are first separately assembled then combined as shown in Fig. 3. The stiffening actuation layer uses selective bonding of TPE (Stretchlon 200, FiberGlast USA) with Teflon as a masking material. The Teflon layer is laser cut into a connected network of Miura-ori shapes and the TPE layers are cut into a rectangular shape using a CO_2 laser cutter (VLS3.75, Universal Laser Systems). The TPE and Teflon are aligned on an aluminum alignment plate and heat pressed for 10 min at 140°C and 700 kPa (Fig. 3A).

The three OSMs are prepared through a series of spin-coating (6800 Spin Coater, Specialty Coating Systems) to create the deformable dielectric. Ecoflex 00-10 is used to coat two separate acrylic plates prior to fabrication to temporarily fix the copper electrodes during the fabrication process. The copper (Pyralux, DuPont) electrodes are cut into the Miura-ori shape using a DPSS laser (Matrix-355, Coherent Inc., CA, USA). Each electrode is aligned on their respective acrylic plates using the stiffening actuation layer as an alignment guide. The acrylic plates are each coated with Ecoflex 00-50 at 900 rpm for 30 s (Fig. 3B). These coated electrodes are set to cure in an oven at 70°C for 20 min. The stiffening actuation layer is then placed on top of one set of copper electrodes. A bonding layer of Ecoflex 00-50 is then coated on the remaining acrylic plate at 1100 rpm for 30 s. The electrodes on this plate are removed to be manually aligned over the stiffening actuation layer as shown in Fig. 3D. The bonding layer is allowed to cure at room temperature for 6 h.

Non-folding sections of the Miura-ori pattern are laser cut from 0.05 mm thick Mylar and aligned on a second Mylar layer which acts as a flexible layer. The two Mylar layers are adhered with pressure sensitive adhesive (467MP, 3M, USA) as seen in Fig. 3C. Areas of the flexible layer not stacked with the Miura pattern have half the thickness of rigid sections and act as folding joints of the pattern.

The OSM-stiffening layer is adhered to the Mylar fold patterns on both sides and the same copper electrode shape is adhered to one side of the Mylar guides to act as the passive shielding mechanism as shown in Fig. 3E. The assembly of layers is then folded manually into the Miura pattern and sealed inside a 9×4 cm outer wrapping of TPE (Fig. 3F). This outer wrapping is sealed with outlets for stiffening actuation, contraction actuation, and for wired connections to each copper electrode on the OSMs. The assembly is then wrapped into an elliptical configuration and sealed using flexible adhesive (Loctite) (Fig. 3G).

III. Sensor Modeling

To obtain a general understanding of the OSM behavior and guide our design, capacitance is first modeled as a function of force. Under a small compressive strain assumption, the one-dimensional stress-strain equations for elastic materials can be substituted into the general equation for capacitance between two electrodes, $C = k\epsilon A/d$, to give

$$\frac{C}{C_0} = 1 + \frac{F}{AE} \tag{1}$$

where C_0 is the initial capacitance under no forces, F is the applied force, A is the surface area of the electrodes given by a and b in Fig. 4A, and E is the dielectric Young's modulus. For modeling OSM folding, it is assumed that the distance, d, between electrodes (Fig. 4B) is governed by geometry near flat folding angles (large α) and by material properties for small α due to compressive stiffening of the dielectric. The flat electrode distance, d_0, causes folding shear strains

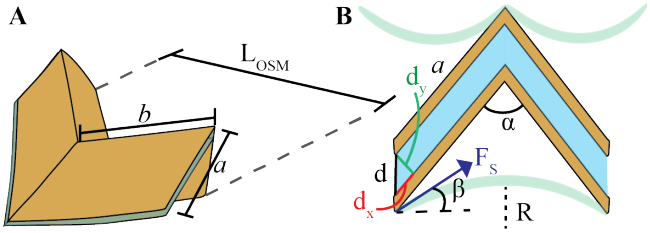

Fig. 4. Sensor modeling. A) An OSM shown in a folded configuration defined by the length L_{OSM}. B) Side view showing the change in d due to folding shear and due to folding compression.

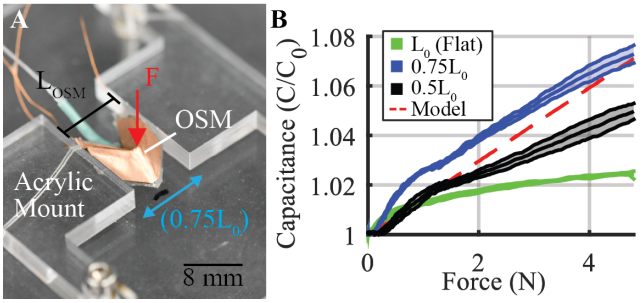

Fig. 5. A) Test setup for mounting OSMs in each configuration. B) OSM force characterization demonstrating an increase in capacitance range over 5 N of force when folded into specific configurations. The dashed line is output from the model, the solid line is the mean from three experiments of one prototype and the shaded region is one standard deviation.

to occur via an increase in lateral distance, d_x, and a small decrease in normal distance, d_y, modeled by

$$d_x = \frac{d_0}{tan(\alpha/2)} \tag{2}$$

$$d_y = \frac{d_0}{(\sqrt{\frac{a+\frac{d_0}{tan(\alpha/2)}}{a}}} \tag{3}$$

For larger α, the magnitude of d increases resulting in a capacitance decrease and a greater range of distances the electrodes can travel due to force.

With small compressive strain, the compressive force that directly affects d due to surface tension, $F_s = \Delta P R b sin(\beta)$, modeled by the Law of Laplace, is related to strain via constitutive relations. Here, ΔP is the difference in pressure across the outer TPE, R is the radius of curvature of the TPE (Fig. 4B), b is one dimension of the origami, and β is the contact angle of the film. The compressive strain is

$$\epsilon_{comp} = \frac{F_s}{AE} \tag{4}$$

where A is the surface area over which compression is applied, in this case $A = a \times b$. This material strain becomes larger than the geometric shear strain for smaller α. Using material strain, the resulting relationship shows that as the OSM is folded (i.e., vacuum pressure is applied), d decreases and thus increases capacitance. As a result, this relation demonstrates that applied force during expansion (i.e., unfolding the pattern) results in larger capacitance than if no forces were applied.

IV. Results and Discussion

The design of the OSM was validated through characterization of capacitance response in a single OSM due to external loading and folding (see Sect. IV-A). Three OSMs were then integrated in the robot (see Sect. II-A.2). Sensor response due to actuation was characterized by measuring capacitance at varying pressures of contraction and expansion of the soft robotic retractor (Sect. IV-B). In measuring the response, we can decouple response due to expansion and response due to force application. The sensor response was then calibrated with respect to the force that is output by the retractor via expansion actuation (Sect. IV-C). Sensor monitoring range was measured to approximate the force output of the retractor at varying actuation pressures and account for initial forces that may be present in a constrained environment. Lastly, in-vitro experiments were performed with a brain tissue model for force-sensing validation (Sect. IV-D).

A. Individual Module Characterization

An OSM was tested in three different folding configurations to demonstrate the force response of the sensor at different module orientations. These configurations were defined as follows: flat ($L_{OSM} = L_0$), folded configuration 1 ($L_{OSM} = 0.75L_0$), and folded configuration 2 ($L_{OSM} = 0.5L_0$). Three trials for each configuration were done using an Instron (5943 Instron, USA) machine to apply 5 N at a rate of 1 mm/min. An acrylic test setup mounted the module in each configuration, as shown in Fig. 5A. The resulting normalized capacitance changes are plotted with the model from Eq. 1 in Fig. 5B.

For each folding configuration, the normalized capacitance follows the general trend of increasing as the load exerted on the OSM increases. This trend indicate applied forces on the OSM decreases the distance between electrodes and thus, increases capacitance, following the expected trend. In the flat configuration, the OSM was least sensitive to force since the capacitance demonstrates asymptotic behavior at forces lower than 3 N. When the OSM is folded to $0.75L_0$, the range of measured capacitance is increased with the same level of applied forces. However, folding further into the $0.5L_0$ configuration, reduces this range. This behavior was repeatably observed over three trials in three prototypes. These results represent how distance between electrodes change with folding and subsequent changes in measured capacitance. The observations also follow trends predicted by our model, where force range increase results from the greater distance an electrode may move when in a folded configuration. Since OSMs are folded in the sensorized retractor, these results validate the OSMs ability to measure forces in the target range (0-5 N) of tissue interaction.

B. Motion Characterization

The sensorized robotic retractor was mounted into an acrylic test setup with its central axis aligned downward (Fig. 6A). An electro-pneumatic circuit (ITV, SMC) controlled the internal pressure of both the vacuum and stiffening

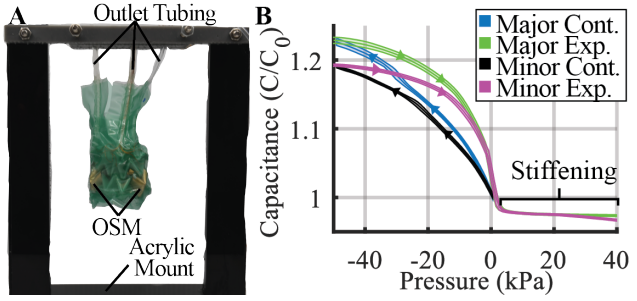

Fig. 6. A) Motion characterization test setup. B) Capacitance response of both major and minor axis OSMs characterized over the full range of motion of the retractor. The solid line represents the mean and the shaded area represents the standard deviation over three trials.

actuation mechanisms. An NI DAQ interfaced with Python simultaneously controlled pressure and collected pressure data. A separate circuit board with a capacitance-to-digital converter (AD7746, Analog Devices) was interfaced to monitor the capacitance of the retractor during pressurization.

The results, shown in Fig. 6B, display capacitance values increasing during contraction to -50 kPa. The capacitance is normalized with respect to the initial configuration at atmospheric pressure (0 kPa). The normalized capacitance behavior generally follows a parabolic behavior becoming asymptotic at full contraction (-50 kPa). This behavior can be attributed to the decrease in folding rate at higher pressures until maximum contraction when the origami pattern is physically constrained. The same behavior is observed in reverse when the retractor expands to atmospheric pressure. When stiffening actuators are pressurized the normalized capacitance decreases from the original value before remaining constant throughout the rest of the stiffening to 40 kPa. Since stiffening causes an initial increase in capacitor plate distance we expect this decrease in capacitance. The constant behavior is due to the retractor not significantly expanding from the atmospheric pressure state; therefore, a similar constant behavior is exhibited by the sensors. While there is an average hysteresis of 15% between contraction and expansion processes, during operation, each process may be treated separately with expansion being the main process where force interactions will be measured. Further, the standard deviation remains small over three trials (Fig. 6B), ensuring accurate measurements within each process.

C. Force Calibration

The capacitance response of each axis was calibrated over a range of 0-5 N to capture the potential forces used for brain retraction [8]. Applied forces were measured during immediate expansion of the retractor from -50 to 0 kPa and stiffening of the retractor to 40 kPa. All capacitances are normalized to the capacitance values at 0 kPa prior to testing. The sensorized robotic retractor was mounted on an acrylic base and a 3D printed curved tip mounted on an Instron was lowered over the major axis of the robot at 0 kPa, as shown in Fig. 7A. Two ATI Nano17 force sensors measure forces output along the minor axis. The robot was then cycled through contraction, immediate expansion, and stiffening pressures. To vary the level of applied forces, the Instron was lowered so that data was collected in 0.1 N increments up to 5 N.

The capacitance is plotted against forces on the major and minor axes in Fig. 7B and 7C, respectively. A calibration curve obtained by a linear fit correlates the output forces to the capacitance response. The calculated sensitivity of the sensor is 0.032 N^{-1} resulting in changes of about 0.25 N that can be accurately measured by our data acquisition setup. This resolution translates to increments of 0.5 kPa in retraction pressure increases that can be presented to inform surgeon decision making. This performance is comparable to commercial intracranial pressure sensors which have resolutions around 0.4 kPa [37]. At full expansion, the retractor is in full contact with the Instron tip, so the area of the tip is used to calculate the applied retraction pressures. Therefore, the OSM meets the desired resolution to detect potential damaging increases to intracranial pressure.

To estimate the force range over varying actuation pressures, the Instron was lowered to the height of the retractor at -50 kPa so that release of the vacuum immediately causes contact. Measurements were collected in 1 kPa steps up to 40 kPa and shown plotted for the major and minor axis in Fig. 7D and Fig. 7E, respectively. In this environment, the forces applied in both axes each achieve a max output of 3.3 N. The normalized capacitance decreases linearly with increases in force over varying pressures. Further, at stiffening pressures, the constant behavior of the force is mirrored by the capacitance. We therefore, estimate the capacitance being linearly related to force over varying pressure within the range of 0 to 3.3 N. Forces greater than 3.3 N are the result of loading an initial force on the retractor at full vacuum simulating a highly constrained environment. The experiment was repeated with the Instron moved -1 mm into the retractor to validate the predicted force (Fig. 7F). In this case, the OSMs overpredict forces with an average error of 0.38 N or 0.55 kPa over the range of actuation pressures.

D. In-Vitro Validation Experiments

A simulated brain tissue model was fabricated using molded gelatin (Knox Gelatin) with a thickness of approximately 20 mm. The tissue model was placed inside a mock anatomical model of a skull to mimic the neurosurgical environment, as shown in Fig. 8A. An ATI Nano17 sensor was mounted in the skull behind the tissue model to measure the force output of the retractor. The retractor was first pulled into max contraction at -50 kPa before inserting it between the skull and the tissue. The robot was then expanded to 0 kPa and stiffened to 40 kPa with steps of 1 kPa/s. The actuation pressure, predicted force (from OSM capacitance), and force output were recorded using the electro-pneumatic control setup, described in Section IV-B.

The resulting comparison of predicted and measured force is plotted in Fig. 8B with residuals shown in Fig. 8C. The retractor predicts a force output on the brain of up to 1.2 N compared to the measured 1 N in this setup. The average

D. Van Lewen, C. Wang, H.C. Lee, A. Devaiah, U. Upahhyay, and S. Russo, "Capacitive Origami Sensing Modules for Measuring Force in a Neurosurgical, Soft Robotic Retractor", in the 2024 International Conference on Robotics and Automation (ICRA 2024).

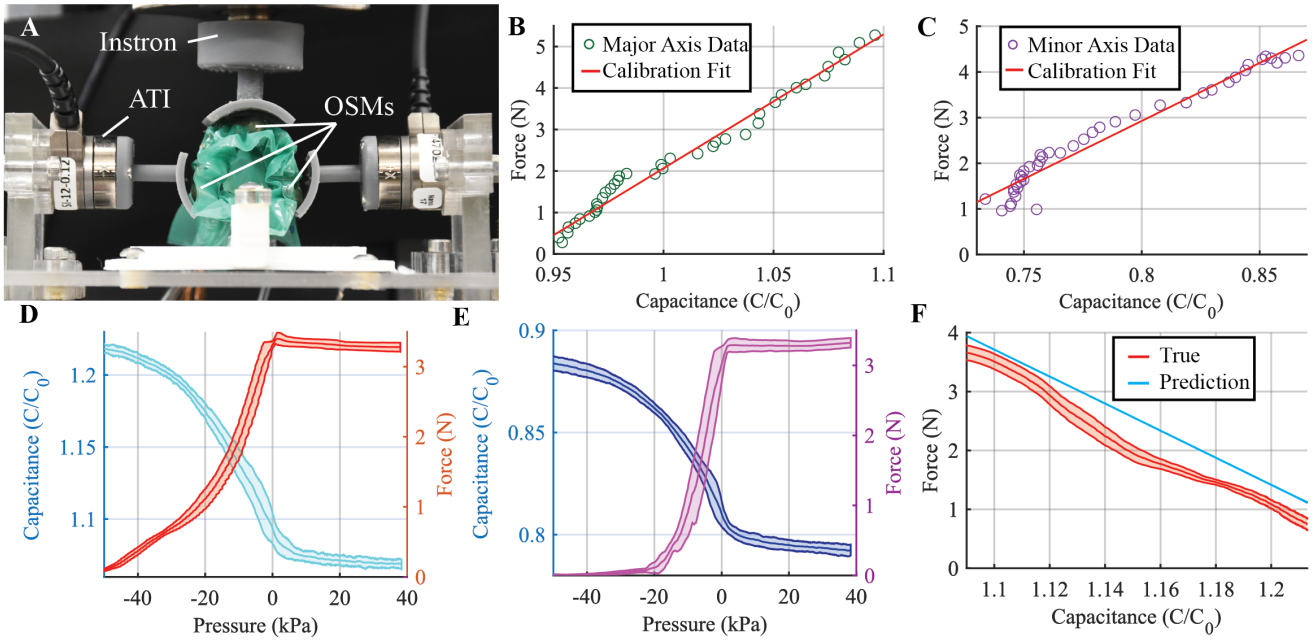

Fig. 7. A) Force calibration measurement setup. B) Capacitance and applied forces at full expansion with fitted calibration curve for major and C) minor axis. D) Capacitance and force over expansion pressures for major and E) minor axis. F) True forces and predicted forces based on calibration. D-F) The solid line is the mean and the shaded region is one standard deviation.

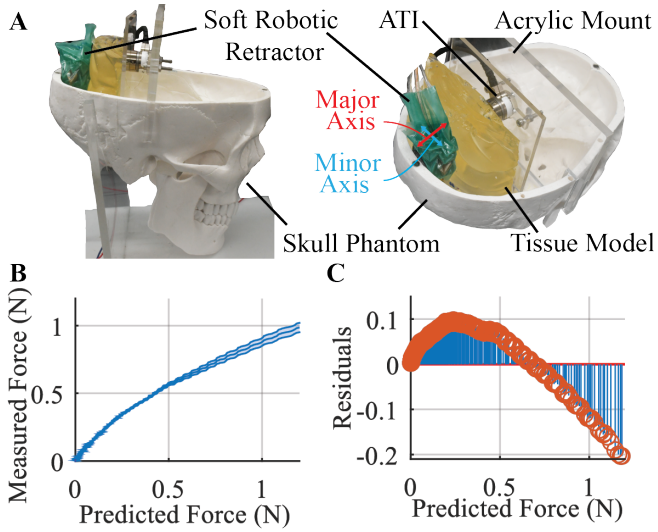

Fig. 8. A) In-vitro experimental setup with gelatin brain tissue model. B) True and predicted forces from in-vitro experiments. C) Residuals.

error in the tissue model is 0.06 N or 5% of the full range with larger forces seeing an overprediction and smaller forces seeing underprediction of forces. The source of error is likely due to the deformability of the tissue model. These results demonstrate the ability of the retractor to accurately measure soft tissue force interactions for feedback to the surgeon.

V. Conclusion

With the rising trend of minimally invasive procedures, neurosurgery stands to benefit significantly from robotic systems. This work introduces a soft, foldable robotic retractor with integrated capacitive sensing for measuring force interactions during neurosurgical procedures. Using layered fabrication techniques enables the creation of a folding OSM that measures force based on changes in capacitance. The OSM has the ability to measure a response over the target range of 0-5 N following trends in the model when in various folded configurations. Folding of the OSM integrated within the soft robotic retractor demonstrates a baseline parabolic response to actuation pressures.

The soft robotic retractor is calibrated up to 5 N to adequately capture forces that may be experienced in neurosurgery which have been measured in the range of 3 N [8]. A sensitivity of 0.032 N^{-1} allows for changes in applied forces on the brain of about 0.25 N. At this resolution, the OSM can provide feedback when retraction may significantly increase intracranial pressures ($\approx$3 kPa) enabling a surgeon to prevent undesired complications [5]. The range of forces output by the retractor and their capacitance response are measured up to 3.3 N on both axes of expansion. A linear relationship between capacitance and force approximates the force output of the retractor at varying actuation pressures. The predicted forces are able to account for any initial forces that may result from a constrained surgical environment. The retractor is further validated in an in-vitro experiment through interaction with a soft brain tissue model. The retractor is able to predict forces on the tissue model within an average error of 0.06 N. Through these force predictions, the retractor facilitates safe tissue interaction during neurosurgery.

The implementation of the actuated Miura origami pattern with the presented capacitive sensing mechanism set a framework for future closed loop feedback control based on force measurements. Future work will focus on in-vivo testing to demonstrate interactions with actual brain tissue.

D. Van Lewen, C. Wang, H.C. Lee, A. Devaiah, U. Upahhyay, and S. Russo, "Capacitive Origami Sensing Modules for Measuring Force in a Neurosurgical, Soft Robotic Retractor", in the 2024 International Conference on Robotics and Automation (ICRA 2024).

REFERENCES

[1] Badie, B., Brooks, N., and Souweidane, M. M., "Endoscopic and minimally invasive microsurgical approaches for treating brain tumor patients," *Journal of Neuro-Oncology*, vol. 69, pp. 209–219, 8 2004.

[2] Assina, R., Rubino, S., Sarris, C. E., Gandhi, C. D., and Prestigiacomo, C. J., "The history of brain retractors throughout the development of neurological surgery," *Neurosurgical Focus*, vol. 36, p. E8, 4 2014.

[3] Siegel, R. L., Miller, K. D., Wagle, N. S., and Jemal, A., "Cancer statistics, 2023," *CA: A Cancer Journal for Clinicians*, vol. 73, pp. 17–48, 1 2023.

[4] Zagzoog, N. and Reddy, K. K., "Modern brain retractors and surgical brain injury: A review," *World Neurosurgery*, vol. 142, pp. 93–103, 2020.

[5] Nourallah, B., Zeiler, F. A., Calviello, L., Smielewski, P., Czosnyka, M., and Menon, D. K., "Critical thresholds for intracranial pressure vary over time in non-craniectomised traumatic brain injury patients," *Acta Neurochirurgica*, vol. 160, p. 1315, 7 2018.

[6] Zhong, J., Dujovny, M., Perlin, A. R., Perez-Arjona, E., Park, H. K., and Diaz, F. G., "Brain retraction injury," *Neurological Research*, vol. 25, pp. 831–838, 2003.

[7] Andrews, R. J. and Bringas, J. R., "A review of brain retraction and recommendations for minimizing intraoperative brain injury," *Neurosurgery*, vol. 33, pp. 1052–1064, 1993.

[8] Aggravi, M., Momi, E. D., DiMeco, F., Cardinale, F., Casaceli, G., Riva, M., Ferrigno, G., and Prattichizzo, D., "Hand–tool–tissue interaction forces in neurosurgery for haptic rendering," *Medical and Biological Engineering and Computing*, vol. 54, pp. 1229–1241, 8 2016.

[9] Konya, B., Dankbaar, J. W., and van der Zwan, A., "Brain retraction injury after elective aneurysm clipping: a retrospective single-center cohort study," *Acta Neurochir (Wien)*, vol. 164, no. 3, pp. 805–809, 2022.

[10] Benedictis, A. D., Trezza, A., Carai, A., Genovese, E., Procaccini, E., Messina, R., Randi, F., Cossu, S., Esposito, G., Palma, P., Amante, P., Rizzi, M., and Marras, C. E., "Robot-assisted procedures in pediatric neurosurgery," *Neurosurgical Focus*, vol. 42, no. 5, p. E7, 2017.

[11] Li, G., Su, H., Cole, G. A., Shang, W., Harrington, K., Camilo, A., Pilitsis, J. G., and Fischer, G. S., "Robotic system for MRI-guided stereotactic neurosurgery," *IEEE Transactions on Biomedical Engineering*, vol. 62, no. 4, pp. 1077–1088, 2015.

[12] Kim, Y., Genevriere, E., Harker, P., Choe, J., Balicki, M., Regenhardt, R. W., Vranic, J. E., Dmytriw, A. A., Patel, A. B., and Zhao, X., "Telerobotic neurovascular interventions with magnetic manipulation," *Science Robotics*, vol. 7, p. 9907, 2022.

[13] Koszowska, Z., Brockdorff, M., da Veiga, T., Pittiglio, G., Lloyd, P., Khan-White, T., Harris, R. A., Moor, J. W., Chandler, J. H., and Valdastri, P., "Independently actuated soft magnetic manipulators for bimanual operations in confined anatomical cavities," *Advanced Intelligent Systems*, p. 2300062, 7 2023.

[14] Blanco, R. G. F. and Boahene, K., "Robotic-assisted skull base surgery: preclinical study," *Journal of Laparoendoscopy Advanced Surgery Technology A*, vol. 23, no. 9, pp. 776–782, 2013.

[15] Gupta, M., Chan, T. M., Santiago-Dieppa, D. R., Yekula, A., Sanchez, C. E., Elster, J. D., Crawford, J. R., Levy, M. L., and Gonda, D. D., "Robot-assisted stereotactic biopsy of pediatric brainstem and thalamic lesions," *Journal of Neurosurgery: Pediatrics PED*, pp. 1 – 8, 2020.

[16] Liu, L., Mariani, S. G., Schlichting, E. D., Grand, S., Lefranc, M., Seigneuret, E., and Chabardès, S., "Frameless rosa® robot-assisted lead implantation for deep brain stimulation: Technique and accuracy," *Operative Neurosurgery*, vol. 19, pp. 57–64, 7 2020.

[17] Burgner, J., Rucker, D. C., Gilbert, H. B., Swaney, P. J., Russell, P. T., Weaver, K. D., and Webster, R. J., "A telerobotic system for transnasal surgery," *IEEE/ASME Transactions on Mechatronics*, vol. 19, pp. 996–1006, 2014.

[18] Kim, Y., Cheng, S. S., and Desai, J. P., "Active stiffness tuning of a spring-based continuum robot for mri-guided neurosurgery," *IEEE Transactions on Robotics*, vol. 34, no. 1, pp. 18–28, 2018.

[19] Gopesh, T., Wen, J. H., Dieppa, D. S., Yan, B., Pannell, J. S., Khalessi, A., Norbash, A., and Friend, J., "Soft robotic steerable microcatheter for the endovascular treatment of cerebral disorders," *Science Robotics*, vol. 6, p. 601, 8 2021.

[20] Song, S., Fallegger, F., Trouillet, A., Kim, K., and Lacour, S. P., "Deployment of an electrocorticography system with a soft robotic actuator," *Science robotics*, vol. 8, p. eadd1002, 5 2023.

[21] Amadeo, T., Van Lewen, D., Janke, T., Ranzani, T., Devaiah, A., Upadhyay, U., and Russo, S., "Soft robotic deployable origami actuators for neurosurgical brain retraction," *Frontiers in Robotics and AI*, vol. 8, p. 437, 1 2022.

[22] Polygerinos, P., Correll, N., Morin, S. A., Mosadegh, B., Onal, C. D., Petersen, K., Cianchetti, M., Tolley, M. T., and Shepherd, R. F., "Soft robotics: Review of fluid-driven intrinsically soft devices; manufacturing, sensing, control, and applications in human-robot interaction," *Advanced Engineering Materials*, vol. 19, pp. 1–22, 2017.

[23] Chen, Y.-W., Pancham, P. P., Mukherjee, A., Martincic, E., and Lo, C.-Y., "Recent advances in flexible force sensors and their applications: a review," *Flexible and Printed Electronics*, vol. 7, no. 3, p. 033002, 2022.

[24] Sareh, S., Jiang, A., Faragasso, A., Noh, Y., Nanayakkara, T., Dasgupta, P., Seneviratne, L. D., Wurdemann, H. A., and Althoefer, K., "Bio-inspired tactile sensor sleeve for surgical soft manipulators," *Proceedings - IEEE International Conference on Robotics and Automation*, pp. 1454–1459, 9 2014.

[25] Rasmussen, E., Guo, D., Murthy, V., Mishra, R., Riviere, C., and Majidi, C., "A soft resistive sensor with a semicircular cross-sectional channel for soft cardiac catheter ablation," *Sensors*, vol. 21, no. 12, p. 4130, 2021.

[26] McCandless, M., Gerald, A., Carroll, A., Aihara, H., and Russo, S., "A soft robotic sleeve for safer colonoscopy procedures," *IEEE Robotics and Automation Letters*, vol. 6, no. 3, pp. 5292–5299, 2021.

[27] Zhao, X.-F., Wen, X.-H., Zhong, S.-L., Liu, M.-Y., Liu, Y.-H., Yu, X.-B., Ma, R.-G., Zhang, D. W., Wang, J.-C., and Lu, H.-L., "Hollow MXene sphere-based flexible e-skin for multiplex tactile detection," *ACS Applied Materials Interfaces*, vol. 13, no. 38, pp. 45 924–45 934, 2021.

[28] Roberts, P., Zadan, M., and Majidi, C., "Soft tactile sensing skins for robotics," *Current Robotics Reports*, vol. 2, no. 3, pp. 343–354, 2021.

[29] Yang, J. C., Mun, J., Kwon, S. Y., Park, S., Bao, Z., and Park, S., "Electronic skin: Recent progress and future prospects for skin-attachable devices for health monitoring, robotics, and prosthetics," *Advanced Materials*, vol. 31, no. 48, p. 1904765, 2019.

[30] Yin, J., Hinchet, R., Shea, H., and Majidi, C., "Wearable soft technologies for haptic sensing and feedback," *Advanced Functional Materials*, vol. 31, p. 2007428, 9 2021.

[31] Kim, U., Lee, D.-H., Yoon, W. J., Hannaford, B., and Choi, H. R., "Force sensor integrated surgical forceps for minimally invasive robotic surgery," *IEEE Transactions on Robotics*, vol. 31, no. 5, pp. 1214–1224, 2015.

[32] Russo, S., Ranzani, T., Walsh, C. J., and Wood, R. J., "An additive millimeter-scale fabrication method for soft biocompatible actuators and sensors," *Advanced Materials Technologies*, vol. 2, p. 1700135, 2017.

[33] Ranzani, T., Russo, S., Schwab, F., Walsh, C. J., and Wood, R. J., "Deployable stabilization mechanisms for endoscopic procedures," *IEEE International Conference on Robotics and Automation (ICRA)*, pp. 1125–1131, 2017.

[34] Russo, S., Ranzani, T., Gafford, J., Walsh, C. J., and Wood, R. J., "Soft pop-up mechanisms for micro surgical tools: design and characterization of compliant millimeter-scale articulated structures," *IEEE International Conference on Robotics and Automation (ICRA)*, pp. 750–757, 2016.

[35] Rogatinsky, J., Gomatam, K., Lim, Z. H., Lee, M., Kinnicutt, L., Duriez, C., Thomson, P., McDonald, K., and Ranzani, T., "A collapsible soft actuator facilitates performance in constrained environments," *Advanced Intelligent Systems*, p. 2200085, 6 2022.

[36] Van Lewen, D., Janke, T., Lee, H., Austin, R., Billatos, E., and Russo, S., "A millimeter-scale soft robot for tissue biopsy procedures," *Advanced Intelligent Systems*, p. 2200326, 1 2023.

[37] Abraham, M. and Singhal, V., "Intracranial pressure monitoring," *Journal of Neuroanaesthesiology and Critical Care*, vol. 2, pp. 193–203, 2015.